Journal of Applied Polymer Science

Mechanical and barrier properties of soy protein isolate films plasticized with a mixture of glycerol and dendritic polyglycerol

Mojca Božič,[1] Martina Majerič,[1] Matjaž Denac,[2] Vanja Kokol[1]

[1]Institute for Engineering Materials and Design, University of Maribor, Smetanova Ulica 17, Maribor SI-2000, Slovenia

[2]Faculty of Economics and Business, University of Maribor, Razlagova 14, Maribor SI-2000, Slovenija

Correspondence to: V. Kokol (E-mail: vanja.kokol@um.si)

ABSTRACT: Soy protein isolate (SPI) films plasticized with different contents of short and linear glycerol (G) and hyperbranched dendritic polyglycerol (DPG) in the presence of water were prepared for the first time with kneading and compression molding; these were analyzed in relation to their visual, morphological, microstructural, mechanical, and water- and oxygen-barrier properties. It was shown that the film prepared with a mixture of 15G15DPG (where the numbers represent the weight percentage of the respective compound) had a higher tensile strength (~14.4%), lower elongation at break (~85.7%), and improved water-barrier (~54.6%) and oxygen-barrier (~84.1%) properties compared to the SPI film plasticized only with 30G. The attenuated total reflectance–Fourier transform infrared spectra of the plasticized SPI films indicated that such properties were related to the approximately 11.3% higher conversion of SPI from the α-helical conformation to the intramolecular β-sheet structures for the 15G15DPG films. This resulted in finer films with lower surface roughnesses and surface areas. On the other hand, further increases in G and DPG revealed an opposite effect and worsened the properties; this was much more pronounced by the increased DPG amount because of SPI unfolding and aggregation and resulted in microporous films. © 2015 Wiley Periodicals, Inc. J. Appl. Polym. Sci. **2015**, *132*, 41837.

KEYWORDS: biopolymers and renewable polymers; packaging; plasticizer; proteins; thermoplastics

Received 8 July 2014; accepted 4 December 2014

DOI: 10.1002/app.41837

INTRODUCTION

The speed of development and the processing of advanced materials is crucial in the achievement of global competitiveness and may represent a revolutionary milestone within the technological developments of the 21st century, where recyclability is an obliged material parameter. Biopolymers based on such natural resources as starch, protein, and cellulose are regarded as attractive alternatives as they are abundant, renewable, inexpensive, environmentally friendly, and biodegradable. In particular, soy protein isolate (SPI), being isolated from oil industry waste, has become an important resource for uses such as fibers, molded-plastic parts, films, and fillers from among a wide variety of products currently supplied by petroleum-based polymers.[1,2] However, the poor mechanical properties and water sensitivities of differently plasticized SPI films and composites have not been resolved thoroughly enough, and despite the strenuous efforts being made,[3] these drawbacks still limit the commercial applications of these materials. It has been reported that water-resistant SPI can be prepared with an organic solution of an alkyl or alkenyl succinic anhydride and by blending it with biodegradable synthetic polymers such as polylactide and polyester. In these cases, the water resistance has been improved, but the problem of biodegradability has again resurfaced as a result of the slow degradation of the synthetic polymers.[4]

The amino-acid composition and molecular weight of the protein, which can vary and be significantly dependent on the type of protein and the experimental parameters used during plastic preparation,[5,6] determines the abilities of SPI chains to interact with each other (via disulfide covalent bonds, hydrogen bonding, electrostatic attractions, and hydrophobic bonding) and with other components of the formulation; this renders its stabilization. SPI mainly consists of acidic amino acids (aspartic and glutamic acids), nonpolar amino acids (alanine, valine, and leucine), basic amino acids (lysine and arginine), and a noncharged polar amino acid (glycine). The secondary structure comprises a mixture of albumins and globulins, 90% of which are storage proteins with globular structures consisting mainly of (in addition to 2S and 15S fractions) 7S (β-conglycinin) and 11S (glycinin) globulin fractions. 11S contains 20 intramolecular disulfide bonds that originate from cysteine residues, whereas disulfide crosslinking in conglycinin is limited because there are only two to three cysteine groups per molecule.[7] During heat processing, the proteins disaggregate, denature, dissociate, unravel, and align toward the direction of the flow.[8,9]

Table I. Components of the Six Studied Formulations of the SPI Plasticized Films

	Proportions (% w/w to SPI dry basis)			
Formulation label	SPI	H2O	G	DPG
70W	100	70	—	—
30G	100	70	30	—
40G	100	70	40	—
50G	100	70	50	—
15G15DPG	100	70	15	15
20G20DPG	100	70	20	20
25G25DPG	100	70	25	25

As native proteins cannot be processed, plasticizers are generally added to the protein matrix to improve its processability and to modify the properties of its final structure. Water is the more effective plasticizer in protein-based materials; however, when thermal processing exceeds a temperature of 100°C, water evaporates and the protein films become brittle. Biocompatible and nontoxic glycerol (G), with its high boiling point (i.e., 290°C) and good stability, is regarded as one of the more efficient plasticizers for SPI plastics. However, as a linear molecule, it possesses three functional groups within the polymer chain, which restricts the possibilities for multihydrogen bonding and the preparation of multibonded protein conjugates. Dendritic polyglycerols (DPGs) with high molecular weights and hyperbranched structures in combination with an exceptionally high number of functional groups, as well as due to their higher thermal and oxidative stabilities, are thus receiving increased attention,[10–12] particularly for biomedical applications.[13]

Therefore, the objective of this work was to determine the effect of DPG on compression-molded SPI films to improve their mechanical and barrier properties. The effects of the DPG concentrations on the SPI secondary structure, mechanical performance, and water-and oxygen-barrier properties were elaborated and compared to the G-blended films.

EXPERIMENTAL

Materials

The soy protein isolate (SPI) ProFam 974 was purchased from the ADM Specialties Division, The Netherlands. It had protein contents of about 90 and 6% of the moisture content. Profam 974's mainly consisted of acidic amino acids, glutamic acid (19.2 wt %), and aspartic acid (11.5 wt %), and approximately 1 wt % cystine; thus, it had an isoelectric point at a pH of approximately 4.6. G with a weight-average molecular weight of 92.09 g/mol (CAS number 56–81-5) and was purchased from Sigma-Aldrich (Slovenia), whereas DPG, with a weight-average molecular weight of 2500 g/mol (CAS number 25618-55-7), was purchased from Nanopartica GmbH (Germany). All of the materials were used as received.

Film Preparation

The mixing of SPI with additives (G, DPG, and water) was carried out within a planetary mixer and yielded a moist powder. The contents and designations of each formulation are detailed in Table I.

The mixtures were stored within sealed glass bags for at least 24 h to ensure the homogeneous distribution of water. Then, kneading was carried out with a torque rheometer (Brabender LTH 300, Germany) at 90°C for 20 min. The effect of the rotor speed on the fusion behavior of the samples was also studied within the range 25–85 rpm. The weights of each batch were kept constant at 65 g. The ram pressure was supplied by a heavy piston of 5 kg; this supplied a ram pressure of about 285 kPa to the formulation by means of a lever arm. For each SPI mixture, the torque versus time data were recorded for each SPI mixture and converted into viscosities, as stated later. Approximately 10 g of the kneaded mixture was then subjected to compression molding at 125°C and 15 MPa for 3 min between two Teflon-coated aluminum plates with a heated hydraulic press (model HP S1 25 160, Litostroj, Slovenia). A 0.25-mm aluminum frame with dimensions of 30 × 30 cm^2 was placed between the two plates to mark the edges of the film and to control the thickness.[14] All of the films were equilibrated at 60% relative humidity (RH) and 20°C for 1 week before testing and kept in sealed plastic bags until testing.

Viscosity Evaluation

The torque rheometer has proven to be a valuable tool for studying multicomponent thermoplastic systems to assess their processing behavior. It measures the viscosity-related torque generated by the resistance of a material to the shearing action of the plasticizing process. The torque and rotor speed data can be converted into viscosity and shear rate with correlations based on the instrument's dimensions.[15] Byler and Daane[16] suggested the following expression for the relationship between the torque (τ) and angular rotor speed (S):

$$\tau = C_0 S^a \tag{1}$$

where C_0 is a constant that depends on the machine's geometry and a is a constant related to the characteristic of the polymer melt. In most cases, a is taken as an equivalent index of the power law index (n) and can be calculated by the slopes of the plots between log τ and log S data. According to Goodrich and Porter,[15] the torque observed within a Brabender mixing chamber is governed by standard rheological properties with the following relationships:

$$\sigma = K_1 \tau \tag{2}$$

$$\dot{\gamma} = K_2 S \tag{3}$$

$$S = (2\pi/60) R \tag{4}$$

where σ is the apparent shear stress, γ is the apparent shear rate, R is the rotor speed used, and K_1 and K_2 are constants that depend on the dimensions of the rheometer. The K_2 constant also depends on n. K_1 and K_2 and can be described as follows:

$$K_1 = \frac{1}{2\pi R_A^2 h} \tag{5}$$

$$K_2 = \frac{2}{nR_A^{2/n}(R_b^{-2/n} - R_c^{-2/n})} \quad (6)$$

where R_b is the inner radius, R_c is the outer radius, R_A is the average radius, and h is the cylinder length. Goodrich and Porter[15] determined the effective dimensions of a Brabender torque rheometer with the results of calibration, and the dimensions were calculated as $R_b = 1.73$ cm, $R_c = 1.985$ cm, $R_A = 1.86$ cm, and $h = 4.76$ cm. Finally, the viscosity can be calculated from the relationship between the viscosity (η), torque, and rotor speed, by the following equation:

$$\eta = \sigma\dot{\gamma} = \frac{K_1\tau}{K_2 S} \quad (7)$$

Differential Scanning Calorimetry (DSC) and Thermogravimetric Analysis (TGA)

DSC and TGA of the protein processed samples were performed with a differential scanning calorimeter (Mettler Toledo 851, Mettler DSC 20 standard cells TC 10 A processor), calibrated with an indium standard. About 15–25 mg of protein sample was weighed in 100-μL DSC aluminum pans, sealed, and tested after 2 h of equilibration. An empty aluminum pan was used as reference. Measurements were carried out with independent duplicate analyses under atmospheric conditions within a temperature range between 25 and 600°C. The testing rate was 10°C/min.

The determination of SPI T_g was done during the second scan. To eliminate water from SPI, 25 mg of bulk SPI sample with 6% moisture content was heated from 25 to 130°C at a heating rate of 5°C/min and cooled down, and then, the measurement was carried out under atmospheric conditions within a temperature range between 25 and 600°C at a testing rate of 5°C/min.

Attenuated Total Reflectance (ATR)–Fourier Transform Infrared (FTIR) Spectroscopy Analysis

ATR–FTIR spectroscopy was used to record the spectra of the protein samples with a PerkinElmer Spectrum One FTIR spectrometer with a Golden Gate ATR attachment and a diamond crystal. The absorbance measurements were carried out within the range 650–4000 cm^{-1} over 16 scans at a resolution of 4 cm^{-1}. All of the measurements were carried out at least in duplicate.

In regard to analysis of the protein's secondary structure contents, the spectra were curve-fitted within 1600–1700 cm^{-1} (amide I) with the Gaussian function. A linear baseline was established for all of the regions analyzed, and the absorbance was normalized with respect to the peak maximum to prevent undesirable intensity variations. Then, the initial values for the peak positions were determined by Fourier deconvolution. All of the data treatments were performed with Peakfit software version 4.12.

Microstructural Analysis

The morphology–microstructures of the SPI processed samples were observed with scanning electron microscopy (SEM). The dried samples were placed on double-sided tape and examined under a microscope (FEI Quanta 200 3D) with backscattered and secondary electron modes at different magnifications of up to 375× and at an intensity of 15 kV.

Surface characterization and quantification of the films was performed with an ImageJ plugin for surface assessment, denominated by the SurfCharJ plugin.[17] The plugin performed three major steps: (1) image alignment of stereo pairs, (2) cross-correlation for finding the displacement between local features, and (3) reconstruction of the surface topography.[18] The height map was generated by the determination of the best match between a local predefined window on the right image and a local window of the left image. The predefined window on the right image scanned the left image within a predefined distance in the x direction and the cross-correlation coefficient for each step was calculated.[19] The cross-correlation coefficient (r) is given by

$$r = \frac{\sum_{i=1}^{Nx'}\sum_{j=1}^{Ny'}(f_{ij} - \bar{f})(g_{ij} - \bar{g})}{N_{x'}N_{y'}\sigma_f\sigma_g} \quad (8)$$

where N_x' and N_y' are the local dimensions of the searching window, f and g are the local gray levels at the local position (i,j), $\bar{f}$ and $\bar{g}$ are the mean gray levels, and σ_f and σ_g are the standard deviations of the gray levels on the left and right local images, respectively. Three surface images were acquired and quantified from each of the film samples.

Mechanical Property Determination

The tensile strength and elongation at breakage were determined according to the ASTM D 638 with a Zwick/Roell ZO 10 instrument at a temperature of 23 ± 2°C and an RH of 50 ± 5% with a velocity of deformation of 10 mm/min and a preloading of 0.1 N.[20] The films were conditioned within a controlled environment chamber at 20 ± 2°C and 65 ± 5% RH for a few weeks before testing. Three replicates were tested for each composition. The film thickness was measured with a manual micrometer (0.01–4.99 ± 0.01 mm, Louis Schopper Leipzing Number 10515). Three thickness measurements at different positions were taken for each specimen, and they were in the range 0.24–0.26 mm for all of the films.

Water Vapor Transmission Rate (WVTR) Determination

The WVTR was determined in accordance with ASTM E 96-95. Film samples (6.3-cm diameter disks that had been conditioned for 24 h) were fixed above aluminum cups, each containing 45 g of calcium chloride. The whole device was weighed and then placed within a climatically controlled chamber (32 ± 2°C and 50 ± 5% RH). The cups were then weighed at regular time intervals, and a linear relationship was obtained between the quantity of water transferred per unit of air and time. Three independent determinations were carried out for each film sample, and the mean of these three values is given as the final result.

Oxygen Transmission Rate (OTR) Determination

Before we measured the OTR, the samples were conditioned at a temperature of 20 ± 2°C and an RH of 65 ± 5% within closed desiccators for 1 week. The constant humidity in the desiccators was achieved by the insertion of a crystallizing dish filled with saturated ammonium nitrate solution. The OTR of the films

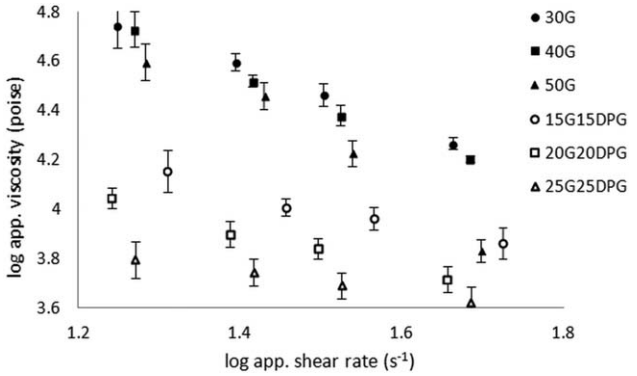

Figure 1. Shear viscosity versus shear rate for SPI mixtures containing different types and quantities of additives (G and DPG) and 70 wt % water at 90°C.

was determined according to ASTM D 3985-06 at 20 ± 2°C and 65 ± 5% RH with an OTR test machine (Mocon Ox-Tran 2/61).The OTR was measured after the film was placed within a cell and the oxygen flow was introduced on one side of the film. The OTR (mL m^{-2} day^{-1}) was calculated from the mean OTR multiplied by the film thickness (mm) and divided by the oxygen gradient within the cell of the testing machine (1 kg f cm^{-2}). Two independent determinations were carried out for each film sample and the mean of these two values is given as the final result.

RESULTS AND DISCUSSION

Rheological Properties

SPIs are composed of long-chain globular molecules; they denature into random coils and break up to some extent in the presence of moisture, heat (i.e., temperatures > 70°C permit the unfolding of the globular structure), and shear experienced during kneading and compression molding.[5,21,22]

Accordingly, the viscosity versus shear rate for all of the SPI formulations were measured at 90°C. The shear stress and shear rate data were determined according to eqs. (2) and (3), respectively, whereas the viscosity was evaluated through the relationship between the shear stress and shear rate according to eq. (7). As shown in Figure 1, the viscosity decreased with increasing shear rate for all of the formulations. The globular protein structures began to align and break during shear deformation, and these broken structures then tended to reform the chains; this depended on the strengths of the applied shear and protein–plasticizer interactions. On the other hand, the viscosity increased with decreasing plasticizer content. It is well-known that plasticizers (i.e., G) reduce the interaction between protein molecules and decrease the mixture viscosity; this decreased the G-content-facilitated charge and polar interactions between the side chains of the SPI molecules, which restricted segmental rotation and molecular mobility.[23] The addition of DPG drastically decreased the viscosities at low rotor speed, but over the share rate of log(1.8 s^{-1}) the viscosity values became substantially similar. G could easily interpose itself between the polymer chains because of linearity, whereas DPG, with its highly branched structure, could not. Thus, the free volume increased and left the SPI molecule in a primary globular state.

Thermal Properties

Figure 2 shows a typical DSC thermogram for SPI, in which two different glass-transition temperatures (T_g), marked as Tg1 at 95.3°C and Tg2 at 132.1°C, were identified; these values corresponded to the low-molecular-weight component, which could have been the 7S globulin, and the higher molecular weight component, which could have been the 11S globulin, respectively. These were consistent with similar DSC curves that have been obtained by a number of researchers,[23–25] who found that the T_g value of the 7S fraction could range from 114 to −67°C and the T_g value of the 11S fraction could range from 160 to −17°C, depending on the moisture contents.

In the characterization of the thermal properties of proteins, a high protein concentration is needed because of the small enthalpic change, whereas the already small content of water present produces major endothermic peaks. The T_g values are thus usually determined by the second run, which may not reflect the real situation occurring during the thermal transitions of proteins as the protein conformations and hydrations of the proteins are inevitably changed after the first scanning run.[26] It was for this reason that the effects of heat denaturation were examined for different SPI mixtures with regard to 70 wt % moisture contents, without the previously performed first run, to determine the water-holding capability depending on the plasticizer type and content. The thermal behaviors of the native SPI and its mixture with G or DPG, respectively, were examined before (Figure 3) and after (Figure 4) kneading and compression molding.

Under controlled conditions of heating rate, the thermal stabilities of the SPI samples could be monitored by the peak transition temperature (T_p), whereas the transformed proportion was reflected by the area under the endothermic peak representing the enthalpy change (ΔH). The sharpness of the transition peak, measured as the width at half-peak height ($\Delta T_{1/2}$), is an index of the cooperative transition from the native to the denatured state.[27] Figure 3 presents the TGA with derivate weight losses and DSC graphs of the dried SPI, SPI with the addition of 70 wt % water, and its mixtures with G, DPG, and water. The high endothermic peaks or weight loss occurring within the region between 20 and 190°C were attributed to residual water loss and represented the energy required to vaporize the water present within the SPI mixtures (Figure 3, right). The same peak masked the T_g values of the 7S and 11S, which were found to be 95.3 and 132.1°C, respectively. It was evident that the broad

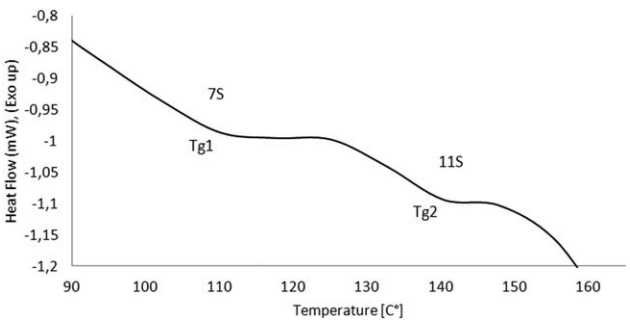

Figure 2. DSC thermogram of the dried SPI powder.

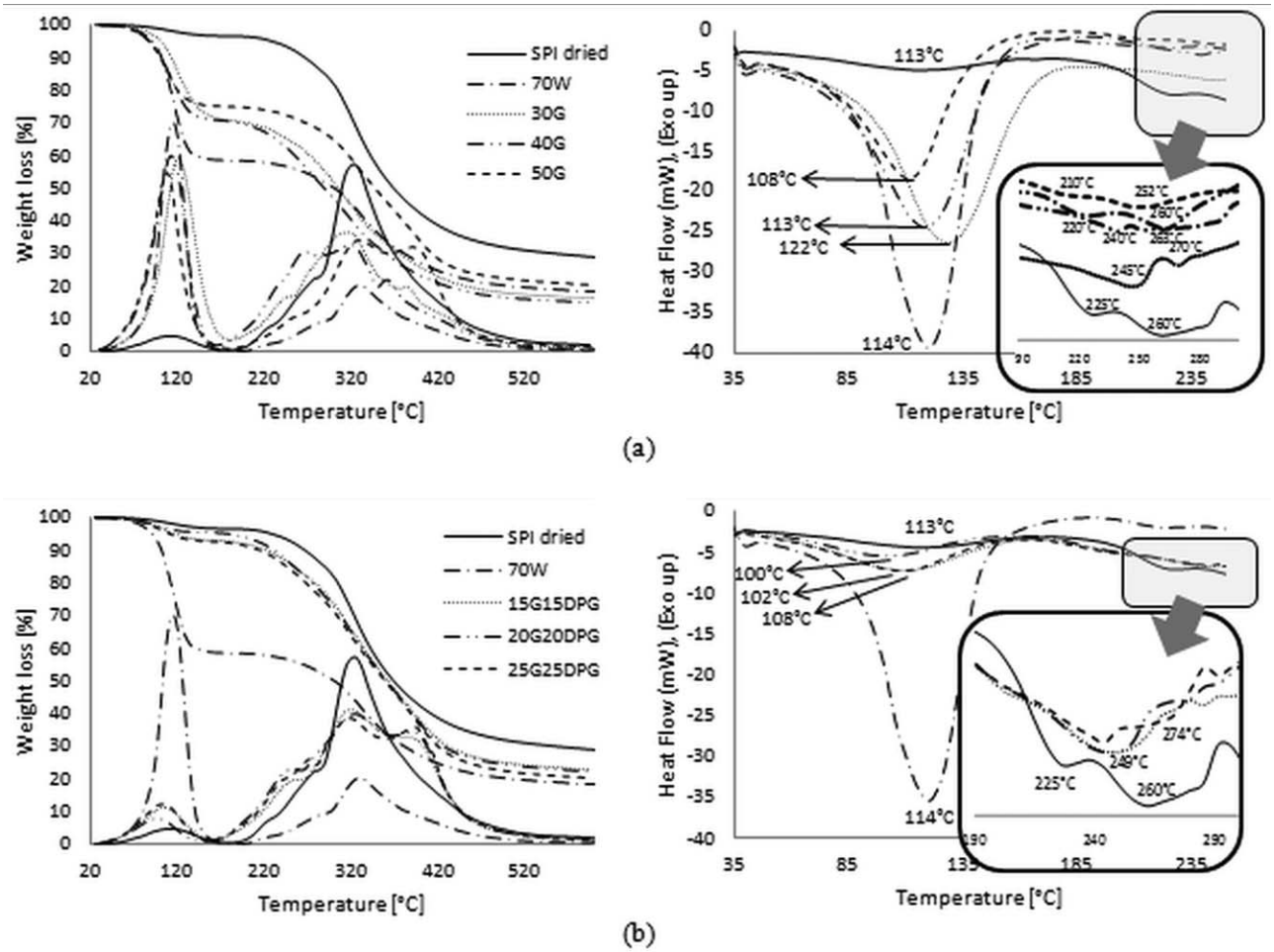

Figure 3. TGA curves with derivative weight losses (left) and DSC curves (right) for SPI and SPI–G–DPG mixtures containing 70 wt % water before temperature kneading and compression molding.

endothermic peak of the reference containing only water (70% w/w) reference compared to the G- and G–DPG-containing SPI mixtures had much higher areas, whereas the difference was even more pronounced for the G–DPG–SPI mixtures. DPG possessed linear OH groups within the core and terminal OH groups on the periphery of the macromolecule. The linear OH groups led to a more polar core of macromolecules, and thus, a high transport of water molecules into the core was observed. Water molecules interacted through hydrogen bonding in the core and yielded very stable supramolecules. This suggested that the water was trapped to a lesser extent within the G-containing SPI mixtures compared to the G–DPG-containing SPI.

The vaporizing transition point (T_p) of the water in the G-containing SPI, determined by the peak value of the endothermic peak, was higher than that of pure water (100°C) and increased from 107.6 to 122.3°C with a decrease in the G content from 50 to 30 wt % (Table II). This indicated that the intermolecular interactions among water, G, and SPI restricted the evaporation of water, and the mixture of 30G seemed to be the more stable. In the case of the G–DPG–SPI mixtures, T_p decreased from 114.2°C for the 70W reference to 90.9°C for the 20G20DPG mixture and to 102.2 and 107.9°C for 25G25DPG and 15G15DPG mixtures, respectively (Table II). These oscillated vaporizing temperatures presented the small content of free, nonbonded water molecules present in the G–DPG–SPI mixtures and could be explained by the different microstructures of the mixtures. This was later confirmed after compression molding, where the produced films, especially the 20G20DPG and 25G25DPG plasticized SPI films, had very irregular microstructures (see the surface morphology properties discussion later).

The second minor endotherms, from 190 to 290°C, were associated with the loss of stable immobilized water, which reflected the molecular mobility of the proteins.[28] The protein chains were organized by the stabilizing effect of so-called immobilized water through hydrogen interactions and thus maintained the formed organization. As shown in Table II, ΔH decreased with increasing content of used G or the mixture of G with DPG; this indicated strong interactions between the additives and water, and thus, water was trapped within the protein matrix. The interactions were especially pronounced in the presence of DPG; this could be explained by the multihydrogen bonds formed between DPG–water and SPI. In addition, the TGA curves of the G–SPI and G–DPG–SPI mixtures indicated a

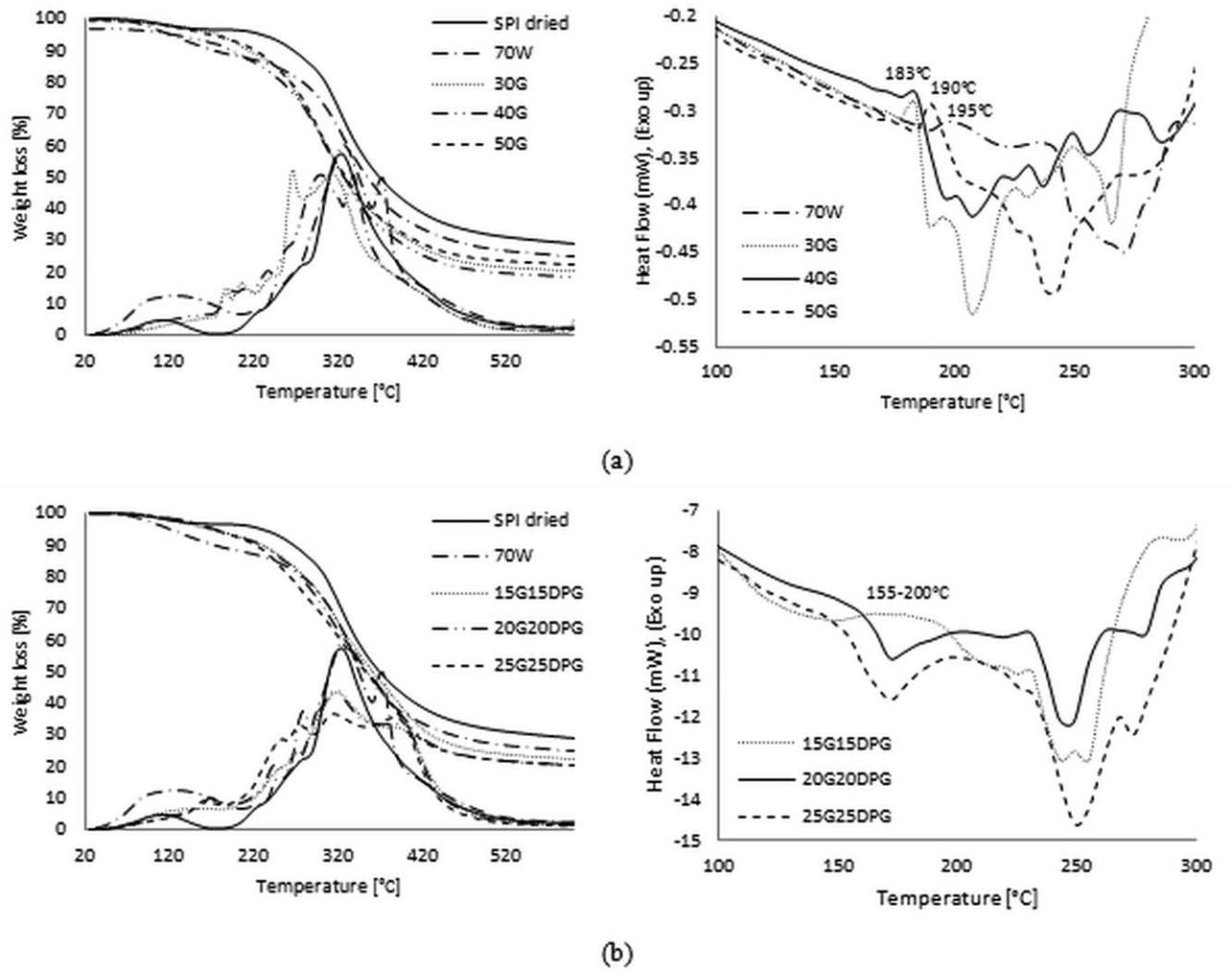

Figure 4. TGA curves with derivative weight losses (left) and DSC curves (right) for SPI–G–DPG films after 20 min of kneading at 25 rpm and 90°C and after compression molding at 125°C and 15 MP for 3 min.

difference between the amounts of residue at 550°C, with the G–DPG–SPI mixtures having a higher amount of residue (~21.7%) compared to the G–SPI mixtures, which had a lower amount of residue (~15.1%). This could have been related to the remaining decomposition products of the DPI and high-molecular DPG.

Table II. Thermal Transition Properties of the Reference SPI (70W) and G–SPI and G–DPG–SPI Mixtures with Constant Water Addition (70 wt %)

	Residual water loss (35–180°C)			Immobilized water loss (190–290°C): ΔH (J/g)[b]	
Formulation	T_p (°C)	ΔH (J/g)	$\Delta H_{1/2}$ (°C)[a]	SPI mixture before kneading and compression molding	SPI film after kneading and compression molding
Native SPI	113.4	105.2	29.4	81.9	
70G	114.2	1452.9	18.8	78.9	1.85
30G	122.3	1052.9	22.7	68.3	3.75
40G	112.7	989.6	21.8	18.8	1.76
50G	107.6	645.2	19.6	26.2	2.36
15G15DPG	107.9	242.4	27.9	34.1	32.7
20G20DPG	90.9	156.8	27.1	32.5	31.5
25G25DPG	102.2	230.1	25.8	16.7	14.5

[a] $\Delta T_{1/2}$ Index of the cooperative transition from the native to the denatured state, measured as the width at half-peak height.
[b] ΔH is the sum of all peak areas between 190 to 290°C because of difficulties in the accurate estimation of the partial areas of individual peaks.

Figure 4 shows the TGA with derivate weight losses and DSC thermographs of the SPI mixtures after they were kneaded at 90°C for 20 min and pressed under 15 MPa at 125° for 3 min. We could clearly see that the profile of the DSC curve for the nonprocessed SPI mixtures (Figure 3) was obviously different from that for the kneaded and compression-molded SPI mixtures. This corresponded to a modification of the new three-dimensional (3D) organization of the protein structure, which was hydrogen-bonded with G and DPG. The change in enthalpy due to the evaporation of the immobilized water (Table II) after the compression molding of the G–SPI mixtures decreased significantly; this indicated high SPI dehydration during thermal compression processing. On the other hand, the enthalpies of the G–DPG–SPI mixtures before and after compression molding were slightly different; this indicated that the water-holding capability was kept almost constant before and after thermal compression processing. These results suggest that the protein chains in the presence of DPG and immobilized water were crosslinked with numerous hydroxyl groups that acted as a new single network, and possible new crosslinked structures were formed with captured water molecules inside. It is also worth noting that for all of the pressed G–SPI mixtures, a sharp exothermic peak occurring at 180–190°C was observed, whereas a broad exothermic peak between 155 and 200°C appeared only in the presence of low DPG addition (i.e., 15G15DPG), and the was not one at higher DPG concentrations. The protein amorphous solid went through thermal aggregation before the endothermic denaturation phase.[8,28] The mechanism of protein association was attributed to interactions such as hydrogen bonding or the association of hydrophobic surfaces. In aqueous dispersions, these protein aggregations are often related to the so-called hydrophobic effect, which is due to the presence of solvent and macromolecular conformations. The addition of the plasticizers can affect the protein aggregations; this depends on the plasticizer type and concentration. In the native state, proteins are typically protected from the free-energy drive toward aggregation, whereas a partially unfolded conformation may determine an intermolecular effective attractive force to minimize the exposure of hydrophobic residues to the polar plasticizers. On the other hand, when the DPG concentration was increased, multihydrogen bonding was increased, and this restricted attractive hydrophobic forces. The multihydrogen bonding of sufficient DPG concentrations with SPI and water molecules reduced the rate of thermal aggregation.

Secondary Structural Analysis

The effect of the plasticizer type and concentration on the secondary structure of soy proteins was investigated by ATR–FTIR spectroscopy. Figure 5 depicts the ATR–FTIR spectra obtained from different plasticized SPI films; they show the characteristic peaks related to C═O stretching at 1630 cm^{-1} (amide I), N—H bending and C—N stretching at 1530 cm^{-1} (amide II), and C—H deformation at 1450 cm^{-1}. The absorption band at 1230 cm^{-1} was attributable to C—N stretching and N—H bending (amide III).[29] Apart from the band at 3500–3000 cm^{-1} related to O—H groups, the typical absorption bands of G and DPG were located within the region from 800 to 1100 cm^{-1}; these corresponded to the vibrations of C—C and C—O.[5] When

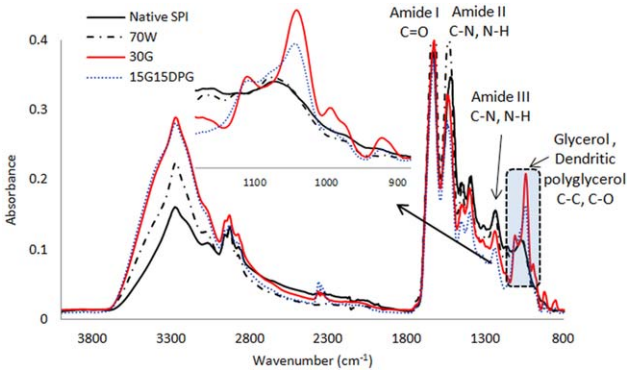

Figure 5. ATR–FTIR absorbance spectra of native SPI and SPI films prepared with 30G and 15G15DPG and containing 70 wt % water. [Color figure can be viewed in the online issue, which is available at wileyonlinelibrary.com.]

comparing the native SPI with the reference (70W) and G- or G–DPG-plasticized SPI, we observed that no obvious change took place in the characteristic peaks of SPI. This indicated that no covalent linkages between the SPI and plasticizers occurred. Some small positional changes in the amide I and II peaks after plasticization and compression molding were attributed to new hydrogen bonding, possibly between the one C═O and two N—H groups.[30]

The amide I region (at about 1630 cm^{-1}) was sensitive to the secondary structure of proteins and could be used to monitor changes in the protein conformation.[29] Through deconvolution of the amide I region, six bands within the 1600–1700-cm^{-1} spectral region were observed (Figure 6): the bands around 1619, 1630, and 1683 cm^{-1} corresponded to the β-sheet structures, whereas the bands around 1644 and 1652 cm^{-1} corresponded to unordered and α-helix structures, respectively, and the bands around 1670 cm^{-1} corresponded to β turns.[31]

Figure 6 displays the deconvoluted ATR–FTIR spectra of the native SPI and the kneaded and compression-molded 70W–SPI, 30G–SPI, and 15G15DPG–SPI mixtures within the amide I

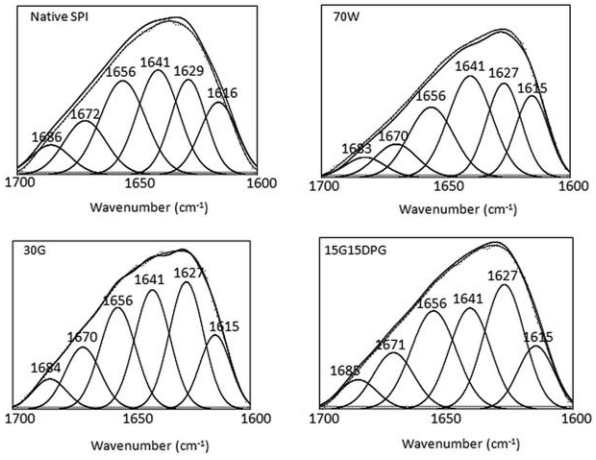

Figure 6. Comparison of the amide I region of the ATR–FTIR deconvoluted absorbance spectra for SPI films prepared with 30G and 15G15DPG and 70 wt % water (constant).

Table III. Protein Secondary Structure Compositions Obtained Through the Deconvolution of the Amide I Region of the atR–FTIR spectra, Mechanical Properties (Tensile Strength and Elongation at Break), and OTR and WVTR Properties of the Native SPI and Differently Plasticized SPI Films

Sample	Protein secondary structure composition (%)			Tensile strength (MPa)[a]	Elongation at break (%)	OTR (mL m^{-2} day^{-1})[b]	WVTR (g mm m^{-2} day^{-1})[c]
	β sheet	α helix, unordered	β turns				
SPI	39.70 ± 1.5	47.68 ± 0.8	12.62 ± 1.0	—	—	—	—
70W	42.82 ± 2.5	48.32 ± 2.7	8.86 ± 2.0	—[d]	—[d]	—[d]	—[d]
30G	43.21 ± 2.1	44.43 ± 0.5	12.32 ± 0.5	9.57 ± 1.8	138.62 ± 10.3	18.2 ± 1.8	177.25 ± 10.8
40G	47.56 ± 2.0	39.56 ± 0.2	12.87 ± 1.0	6.48 ± 0.9	142.89 ± 9.7	19.5 ± 1.1	313.10 ± 9.6
50G	42.40 ± 1.5	44.69 ± 1.0	12.90 ± 1.0	4.82 ± 0.9	188.36 ± 11.9	22.4 ± 1.1	402.42 ± 25
15G15DPG	47.67 ± 0.5	40.45 ± 0.6	11.88 ± 1.5	10.98 ± 2.5	19.75 ± 10.9	2.9 ± 0.6	77.06 ± 4.6
20G20DPG	39.22 ± 0.7	46.30 ± 1.0	14.46 ± 2.0	5.31 ± 1.3	17.99 ± 12.8	10.4 ± 3.3	120.12 ± 8.5
25G25DPG	41.39 ± 1.2	46.46 ± 1.0	12.14 ± 1.5	3.27 ± 0.8	6.79 ± 5.7	29 ± 6.6	200.36 ± 24.6

[a] The mechanical test procedure (tensile strength and elongation at break evaluation) was performed according to ASTM D 638.
[b] WVTR tests were performed at 32 ± 2°C and 50 ± 5% RH according to the ASTM E 96-95 standard. The measured values were normalized to a 1-mm film thickness.
[c] OTR tests were performed at 20 ± 2°C and 65 ± 5% RH according to ASTM D 3985-06. The measured values were normalized to a 1-mm film thickness.
[d] Samples could not be measured because they were too brittle and cracked.

band region (1560–1700 cm^{-1}). For native SPI, two main structures resulted from α-helix/unordered and β sheets; these corresponded to percentage areas of around 47.7 and 39.7%, respectively (Table III). The addition of 70 wt % water as the only plasticizer, combined with the compression-molding treatment, induced mainly the transformations of β turns to β-sheet structures, where the percentage area of the α helix stayed more or less the same. After compression molding with 30 wt % G plasticizer, additional intramolecular β-sheet structures were formed (∼1% increase) compared to the reference (70W). This was due to the conversion of the secondary structure contents of the protein from the α helix/unordered structure. The addition of 30 wt % G did not influence the β-turn percentages. When 15 wt % G with 15 wt % DPG was used as the plasticizer, the conversion of the intramolecular β-sheet structures was higher (∼12.3%) when compared to the 30G sample. Also, in the presence of the DPG, the main part of the transformation was from α helix/unordered to β-sheet structures. The difference in conversion share was attributed to the plasticizers structure. G was a small, linear molecule, which could easily interpose itself between the polymer chains and increase their mobility; thereby, it improved the flexibility and extensibility of the film. On the other hand, only the optimal concentration of DPG together with G promoted a higher share of the protein structure unfolding and, consecutively, refolded it into new intramolecular β-sheet structures.

Table III shows the area percentage contributions of the ATR–FTIR deconvoluted absorbance bands within the amide I region for the native SPI and differently plasticized SPI films. The results suggest that an increase in the G concentration (from 30 to 40 wt %) increased the conversion of the α helix/unordered structure, with a small part of the β turns turned into the intramolecular β-sheet structures, whereas at 50 wt % G, the opposite effect was observed. At high G concentrations, the dipole moment was high enough to induce disruption of the internal hydrogen bonds of the peptide groups by competition between the G—OH group and the peptide N—H group for hydrogen bonding to the amide C═O, and the low dielectric constant of G was able to perturb the structure of protein by reducing the hydrophobic effect. This latter effect promoted the unfolding of the protein and its refolding into an α-helical conformation, which is known as the most energetically stable conformation of proteins.[32] When DPG was included within the G–SPI system, the structural changes were consistent, with a reorganization of the secondary structure of the protein in which the α-helical content dominated, except when 15 wt % G with 15 wt % DPG was applied. When the DPG concentration was increased, the SPI molecular motion and unfolding during kneading and compression molding was decreased; this increased the α-helix content within the formed SPI films. A concentration of 15 wt % G with 15 wt % DPG seemed to be optimal for a balanced content between the α-helix and β-sheet structures.

Mechanical, WVTR, and OTR Properties of the SPI Compression-Molded Films

The mechanical and barrier properties of the reference (70W) film without G and DPG could not be measured because they were too brittle, and there was cracked equipment, so only the other films containing G and/or DPG were analyzed and compared relative to these properties. As shown in Table III, the tensile strength and elongation at breaking for the 30G film were approximately 9.6 MPa and approximately 138.6%, respectively. The increase in G from 30 to 50 wt % caused a decrease in tensile strength (from ∼9.6 to ∼4.8 MPa), and an increase in the elongation at break (from ∼138.6 to ∼188.4). The three hydroxyl groups of G could interact with the amino acid side groups of the protein and, thus, decrease the intermolecular and intramolecular interactions between the protein chains, such as hydrogen bonds; this improved the motion abilities of the protein macromolecules, which resulted in the flexibilities of materials.[7] As a result, the SPI films changed from firm to

highly flexible with increasing G concentration. When we compared the tensile strengths of the G–DPG-containing SPI films, it was obvious that a small addition of 15 wt % DPG helped to improve the tensile strength (~11 MPa) of the films when compared to that of 30 wt % of the total amount of the plasticizer. Through the thermal kneading and compression molding of the SPI films, two kinds of events were initiated: during the kneading phase, the protein structure was disrupted, some native disulfide bonds were cleaved, and sulfhydryl and hydrophobic groups were exposed, whereas during compression molding, a film network through new disulfide crosslinking, new hydrophobic bonds, and also new hydrogen bonds was formed.[33,34] The presence of DPG in the SPI film obviously affected the organization of the protein network during thermal kneading; the protein structure was not disrupted to such a high level compared to the G–SPI films, and thus, globular proteins tended to agglomerate at a high concentration of DPG and form a rough microstructure with the presence of microholes. However, with the appropriate DPG concentration, new multihydrogen interactions between the protein chains surrounded by the DPG molecules could be created during compression molding; this led to an increase in the stability of the protein matrix. With increasing DPG concentration above 15 wt %, both the tensile strength and elongation decreased drastically at breaking. This indicated that because of the SPI uneven heterogeneous distribution within the DPG and, thus, the formation of SPI agglomerations (a high level of globular structures), DPG did not act as a hydrogen-bonding agent with SPI; this led to a highly rough surface microstructure and, in the end, to decreased mechanical properties.

The SPI films were further analyzed in relation to the WVTR and OTR properties (Table III). SPI is hydrophilic in nature, and hence, SPI-based films have high WVTRs. The moisture-barriers properties could be improved by the presence of various crosslinkers or hydrophobic compounds, including aldehydic compounds (i.e., glutaraldehyde, formaldehyde, glyoxal) and epoxy and phenolic compounds,[35] but because of their cytotoxicities, they are restricted from use in food coverings. Therefore, new nontoxic alternatives need to be searched for intensively.

As depicted in Table III, the increase in G from 30 to 50 wt % in SPI mixtures increased WVTR from approximately 177.2 g mm m^{-2} day^{-1} to approximately 402.4 g mm m^{-2} day^{-1} and the OTR values from approximately 18.2 g mm^{-2} day^{-1} to approximately 22.4 g mm^{-2} day^{-1} (both normalized to a 1 mm thickness). Measurements were taken at a relatively high humidity (i.e., WVTR at 50% RH and OTR at 65% RH), where water can increase the polymer free volume. This allowed the polymeric chain segments to increase their mobility[3] and, consequently, increase the mobility of water molecules throughout the films. This strongly enhanced the moisture absorption rates and permeabilities of the SPI films. Nevertheless, these are hard to compare when taking into account the different mixture recipes, preparation methods (casting, molding, etc.), drying conditions, and so on.

The presence of DPG within the G–SPI mixtures resulted in a decrease of both WVTR to approximately 77.1 g mm m^{-2} day^{-1} and OTR to approximately 2.9 mL m^{-2} day^{-1} at a concentration of 15 wt % DPG, whereas higher concentrations (i.e., 25 wt %) increased the WVTR and OTR values up to approximately 200.4 g mm m^{-2} day^{-1} and approximately 29.0 mL m^{-2} per day^{-1}, respectively. The presence of optimal DPG highly increased the entanglement of the network by increasing the level of hydrogen interaction between SPI, G, and DPG. This resulted in a decrease in the free hydrophilic functional groups available for the water to absorb. This led to reduced interstitial spacing among the SPI molecules, which is a measure of the free volume and determines the mass permeability. A decrease in the free volume of the SPI matrix increased the tortuosity of the water molecule pathway through the network, with a consequent decrease in WVTR. In addition to the polymer origin and plasticizers, the diffusivity of water was also strongly influenced by the microstructures of the materials. The existence of compact aligned proteins with continually smooth surfaces restricted the diffusivity of water, whereas rough surfaces with holes readily absorbed water, which could easily penetrate through the thinner parts of the films.

When we considered the fact that OTR measurements were even performed at higher RH (i.e., 65%), an excellent accomplishment was obtained for the 15G15DPG sample. It is well-known that high temperatures and humidity promote a high gas transference across the film in an exponential way. For instance, at RHs below 50%, the oxygen permeability remains quite constant; however, for RHs above 50%, the oxygen permeability can increase exponentially.[36,37] However, the trend of increasing WVTR and OTR was observed for 20G20DPG and 25G25DPG and was attributed to the poor organization of DPG within the SPI network; this caused the SPI aggregation and, through this, the formation of multiple microholes. Gas molecules were absorbed and dissolved into the solid polymer phase and diffused in the solid phase throughout the film. Diffusion occurred in the pores and along the material surfaces. Factors such as high interactions between the permeating molecules and the polymer and the high porosity of the film increased the solubility of the gas molecules.[38]

Surface Morphological Properties

The photographs and SEM images of the SPI films plasticized with only water and G or G–DPG, as presented in Figure 7(a,b). It was apparent that the use of only water as a plasticizer at 70 wt % resulted in very fragile films, which were too brittle to be further handled. Yellow, transparent, flexible SPI films plasticized with 30–50 wt % G could be produced smoothly without cracks and microholes. On the other hand, DPG with a highly branched globular shape could not impose between the SPI chains and, thus, could not sufficiently disrupt the protein-chain hydrogen bonding. However, by through optimization of the G-to-DPG concentration, a smooth and homogeneous surface was obtained. At concentrations of 15 wt % G with 15 wt % DPG, a good dispersion within SPI was achieved. At higher DPG contents (20 and 25 wt %), microsized holes were formed; this indicated that the molecules of SPI with a high DPG content could not sufficiently become entangled, even when a high compression pressure of 15 MPa was used. On the other hand,

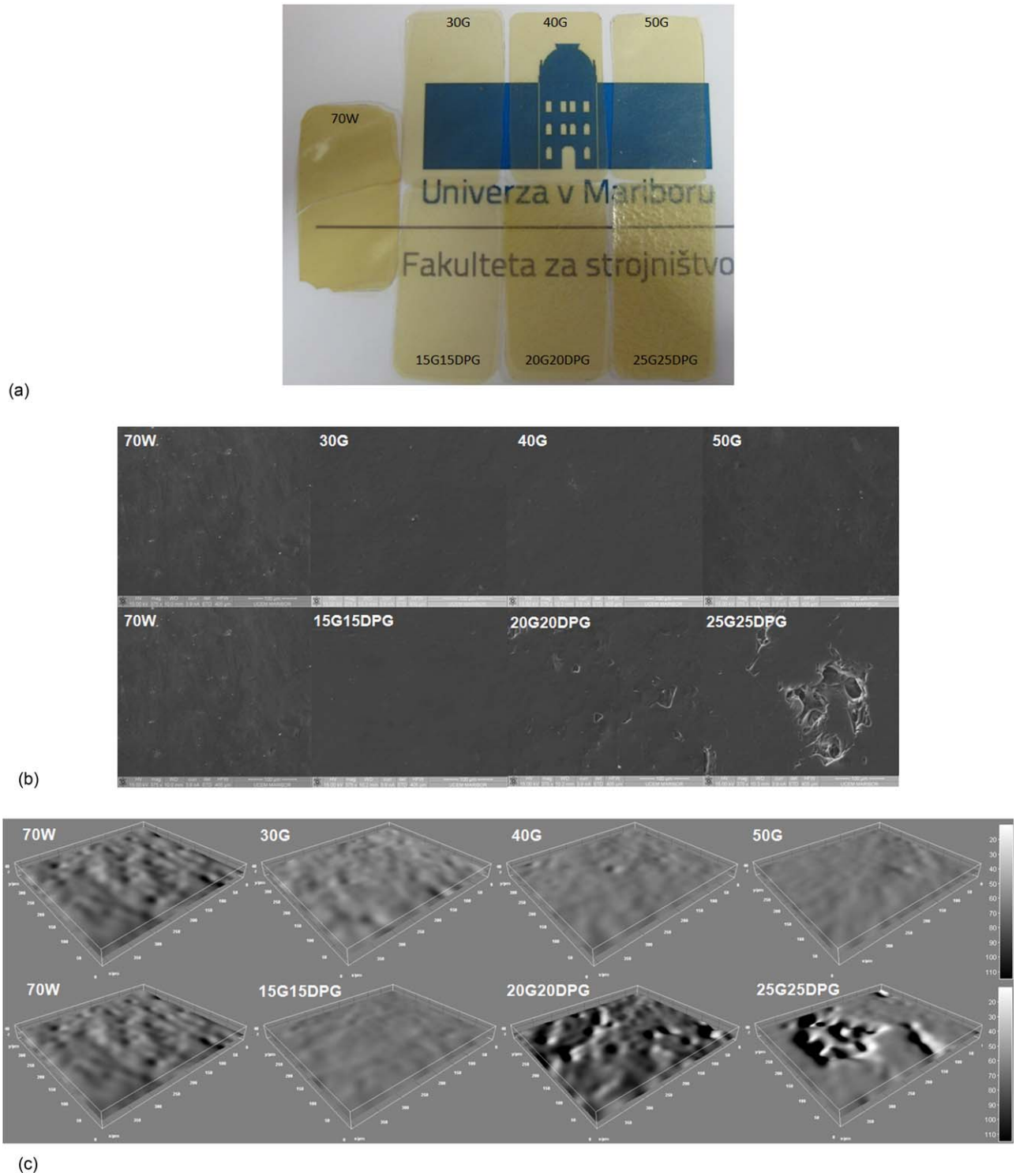

Figure 7. (a) Photographs, (b) SEM surface images, and (c) 3D surface plot images (showing corresponding height maps) of the SPI film surfaces prepared with different G and G–DPG contents kneaded at 90°C for 15 min and pressed at 125°C for 3 min under 150 bar. [Color figure can be viewed in the online issue, which is available at wileyonlinelibrary.com.]

this could offer us the opportunity to design SPI films with controlled microholes.

To provide an objective and effective quantification of the microstructure, a computerized and automatic image analysis was carried out. Figure 7(c) shows the microstructure of the reference 70W and differently plasticized SPI films after compression molding. The (70W) reference film had a granular structure and more voids compared to each of the G-plasticized SPI films and 15G15DPG SPI film. Water alone as a plasticizer was insufficient for enabling the formation of smooth surfaces.

Table IV. Quantification of the Surface Reconstructed Areas Shown in Figure 7(b,c)

Film sample	Roughness (μm)	Surface area (calibrated units of $\mu m^2/\mu m^2 = 1$)
70W	2.72 ± 0.31	3.61 ± 0.23
30G	1.79 ± 0.15	2.64 ± 0.17
40G	1.64 ± 0.11	2.39 ± 0.15
50G	1.59 ± 0.11	2.35 ± 0.14
15G15DPG	1.14 ± 0.10	1.71 ± 0.15
20G20DPG	4.56 ± 0.43	4.49 ± 0.33
25G25DPG	4.67 ± 0.47	4.53 ± 0.39

As the temperature increased to 125°C, the water was evaporated from the SPI matrix; this resulted in irregularities and voids during the continuous protein phase. SPI films plasticized with G yielded smooth and continuous structures, whereas an increased concentration of G enhanced the smoothness trend. On the other hand, the additions of higher concentrations of DPG induced uneven surfaces and the formations of microholes (see samples 20G20DPG and 25G25DPG). The detailed structures of such complexes between DPG and SPI were complicated because of numerous possible interactions between different parts of the SPI molecules. The optimal DPG concentration (i.e., sample 15G15DPG), on the other hand, enabled the compression molding of continually smooth SPI films without the formation of cracks or holes.

The quantification of the surface structures (roughness and surface area) exemplified in Figure 7(b,c) were quantified with the SurfCharJ plugin;[17] the calculated surface area was normalized with the projected areas of the assessed regions having units of $\mu m^2/\mu m^2 = 1$. The results given in Table IV correspond to the mean value of three different images from each of the film samples. The roughness values of the G-plasticized SPI films were similar and varied from 1.8 to 1.6 μm for samples plasticized with 30–50 wt % G, respectively; this indicated similar height variations at the assessed scale. This was also confirmed with similar surface area values, which ranged from 2.6 to 2.3. In the case of the reference 70W film, the roughness and the surface area increased to 2.7 and 3.6 μm, respectively. Films plasticized with a mixture of G and DPG had a wide range of roughness values, which varied from 1.1 to 4.7 μm for plasticized samples 15G15DPG to 25G25DPG, respectively. In addition, the surface area increased from 1.7 to 4.5. The obtained surfaces of the 20G20DPG and 25G25DPG plasticized SPI films were rough and uneven in comparison with the 15G15DPG SPI plasticized film; this resulted in an optimal continually smooth film with the lowest roughness of 1.1 μm.

CONCLUSIONS

SPI plasticization with G and DPG was studied as an innovative, sustainable, and recyclable method for use in the preparation of films for applications such as food packaging, in which high oxygen and water vapor barriers are prerequisites for preserving the qualities of the products. Together with other factors, such as SPI and plasticizer concentrations and kneading with compression molding, DPG influenced the film properties by affecting the unfolding and aggregation mechanisms of the SPI proteins and, thus, changing the distributions of secondary protein structures within the film network. However, with appropriate DPG concentrations within the mixtures with G, the provided films were less permeable to water vapor and oxygen and had good tensile properties but reduced elongation at break values compared to the SPI plasticized with only G. Further research is needed to optimize all of the film properties.

ACKNOWLEDGMENTS

This work was financially supported by a European Union funded 7FP project (NMP4-LA-2012–280759-NanoBarrier). The authors are also grateful to Alexander Kristiansen (SINTEF Materials and Chemistry Institute) for the OTR analysis.

REFERENCES

1. Amar, K. M.; Manjusri Misra, L. T. D. Natural Fibers, Biopolymers, and Biocomposites; Taylor & Francis: New York, **2005**.
2. González, A.; Alvarez Igarzabal, C. I. *Food Hydrocolloids* **2013**, *33*, 289.
3. Song, F.; Tang, D.-L.; Wang, X.-L.; Wang, Y.-Z. *Biomacromolecules* **2011**, *12*, 3369.
4. Kumar, R.; Zhang, L. *Biomacromolecules* **2008**, *9*, 2430.
5. Guerrero, P.; de la Caba, K. *J. Food Eng.* **2010**, *100*, 261.
6. Ciannamea, E. M.; Stefani, P. M.; Ruseckaite, R. A. *Food Hydrocolloids* **2014**, *38*, 193.
7. Guerrero, P.; Retegi, A.; Gabilondo, N.; de la Caba, K. *J. Food Eng.* **2010**, *100*, 145.
8. Nishinari, K.; Fang, Y.; Guo, S.; Phillips, G. O. *Food Hydrocolloids* **2014**, *39*, 301.
9. Hernandez-Izquierdo, V. M.; Krochta, J. M. *J. Food Sci.* **2008**, *73*, 30.
10. Kainthan, R. K.; Brooks, D. E. *Bioconjugate Chem.* **2008**, *19*, 2231.
11. Wilms, D.; Stiriba, S.-E.; Frey, H. *Acc. Chem. Res.* **2010**, *43*, 129.
12. Calderón, M.; Quadir, M. A.; Sharma, S. K.; Haag, R. *Adv. Mater.* **2010**, *22*, 190.
13. Frey, H.; Haag, R. *J. Biotechnol.* **2002**, *90*, 257.
14. Pustak, A.; Pucić, I.; Denac, M.; Švab, I.; Pohleven, J.; Musil, V.; Šmit, I. *J. Appl. Polym. Sci.* **2013**, *128*, 3099.
15. Goodrich, J. E.; Porter, R. S. *Polym. Eng. Sci.* **1967**, *7*, 45.
16. Blyler, L. L.; Daane, J. H. *Polym. Eng. Sci.* **1967**, *7*, 178.
17. Chinga, G.; Johnsen, P. O.; Dougherty, R.; Berli, E. L.; Walter, J. Q. *J. Microsc.* **2007**, *227*, 254.
18. Chinga-Carrasco, G.; Johnsen, P. O.; Øyaas, K. S. *Micron* **2010**, *41*, 648.
19. Gonzalez, R. C.; Woods, R. E.; Hall, P. *Digital Image Processing*, Prentice Hall, New Yersey.

20. Denac, M.; Musil, V.; Šmit, I.; Ranogajec, F. *Polym. Degrad. Stab.* **2003**, *82*, 263.
21. Ralston, B. E. Soy Protein Plastics: Material Formulation, Processing and Properties; ProQuest: Eisenhower Parking, **2008**.
22. Mo, X.; Sun, X. S.; Wang, Y. *J. Appl. Polym. Sci.* **1999**, *73*, 2595.
23. Zhang, J.; Mungara, P.; Jane, J. *Polymer* **2001**, *42*, 2569.
24. Morales, A.; Kokini, J. L. *Biotechnol. Prog.* **1997**, *624*, 13.
25. Kumar, R.; Choudhary, V.; Mishra, S.; Varma, I. K. *J. Therm. Anal. Calorim.* **2004**, *75*, 727.
26. Rouilly, A.; Orliac, O.; Silvestre, F.; Rigal, L. *Polymer* **2001**, *42*, 10111.
27. Li, S.; Wei, Y.; Fang, Y.; Zhang, W.; Zhang, B. *J. Therm. Anal. Calorim.* **2013**, *115*, 1633.
28. Tang, C.-H.; Choi, S.-M.; Ma, C.-Y. *Int. J. Biol. Macromol.* **2007**, *40*, 96.
29. Kong, J.; Yu, S. *Acta Biochim. Biophys. Sin.* **2007**, *39*, 549.
30. Barth, A.; Zscherp, C. Q. *Rev. Biophys.* **2002**, *35*, 369.
31. Elmore, D. L.; Smith, S. A.; Lendon, C. A. *Spectroscopy* **2007**, *22*, 38.
32. Subirade, M.; Kelly, I.; Guéguen, J.; Pézolet, M. *Int. J. Biol. Macromol.* **1998**, *23*, 241.
33. Wittaya, T. Protein-Based Edible Films: Characteristics and Improvement of Properties; INTECH Publishers: Croatia, **2012**.
34. Routray, M.; Rout, S. N.; Mohanty, G. C.; Nayak, P. L. *J. Chem. Pharm. Res.* **2013**, *5*, 752.
35. González, A.; Strumia, M. C.; Alvarez Igarzabal, C. I. *J. Food Eng.* **2011**, *106*, 331.
36. Ma, X. F.; Chen, M.; Meng, K.; Li, F. F. *Adv. Mater. Res.* **2011**, *380*, 270.
37. Pereira, R. N.; Souza, B. W. S.; Cerqueira, M.; Teixeira, J.; Vicente, A. *Biomacromolecules* **2010**, *11*, 2912.
38. Paunonen, S. *BioResources* **2013**, *8*, 3098.